

PERFORMANCE ANALYSIS OF SOLAR ASSISTED MULTIGENERATIONAL SYSTEM USING THERMINOL VP1 BASED NANOFLUIDS A Comparative Study

by

**Muhammad Sajid KHAN^a, Khuram P. AMBER^b,
Hafiz Muhammad ALI^{c*}, Muhammad ABID^d,
Tahir A. H. RATLAMWALA^e, and Samina JAVED^f**

^a Institute of Energy and Power Engineering, Zhejiang University of Technology, Hangzhou, Zhejiang

^b Department of Mechanical Engineering,

Mirpur University of Science and Technology (MUST), Mirpur, Pakistan

^c Mechanical Engineering Department, King Fahd University of Petroleum and Minerals, Dhahran, Saudi Arabia

^d Department of Energy Systems Engineering, Faculty of Engineering, Cyprus International University, Northern Cyprus, Turkey

^e Department of Engineering Sciences,

National University of Science and Technology (NUST), Karachi, Pakistan

^f Department of Mechanical Engineering, University of Engineering and Technology, Taxila, Pakistan

Original scientific paper

<https://doi.org/10.2298/TSCI180608062K>

The application of the nanofluids is suggested to enhance and improve the efficiency of solar thermal power system. In the present study, three different nanofluids (Fe₂O₃/therminol VP1, SiO₂/therminol VP1, and Cu/therminol VP1) are numerically investigated in parabolic dish solar collector that is further integrated to a combined cycle for power and hydrogen production. Heat rejects from the power cycle is also utilized to drive a single effect absorption (LiBr-water) system. Furthermore, a comprehensive energy, exergy and exergo-environmental analysis are carried out by varying several input parameters and their influence on overall energetic and exergetic efficiencies, network output and rate of hydrogen generation is assessed. The engineering equation solver is employed to conduct the parametric study. Outcomes of the study demonstrate that the SiO₂/VP1 has the better characteristics among the investigated nanofluids. The overall energetic efficiency of the SiO₂/VP1, Fe₂O₃/VP1, and Cu/VP1 is almost 38.79%, 38.74%, and 37.53%, while overall exergetic efficiency is 41.72%, 41.66%, and 40.36%, respectively at 1000 Wm⁻². The exergoenvironmental impact coefficient and impact index are noticed to be reduced for all the three nanofluids as mass-flow rate increases. The hydrogen production rate for SiO₂/VP1 is maximum and has observed to be increased by increasing the ambient temperature. Increase in nanoparticles concentration also rises the exergetic efficiency but reduces the thermal conductivity of the nanofluids. Coefficient of performance is noticed to be increased with rise in evaporator temperature, whereas, it is reduced by increasing the generator temperature.

Key words: parabolic dish, exergo-environmental, hydrogen, nanofluids

* Corresponding author, e-mail: hafiz.ali@kfupm.edu.sa; h.m.ali@uettaxila.edu.pk

Introduction

The application of renewable energy resources (especially solar) is the best solution to tackle the environmental threats (CO, CO₂ emissions, depletion of ozone, *etc.*) that are due to the burning of conventional energy fuels. Therefore, energy demand for the society through sustainable and clean recourses is the prime and the most important challenge [1]. The concentrated solar power systems are used for high temperature applications and parabolic dish collector has the highest solar to thermal conversion efficiency [2]. Le Roux *et al.* [3] proposed a rectangular cavity dish receiver model applied as a heat source for Brayton cycle. An experimental and numerical study on the cavity receiver of dish collector was performed by Qiu *et al.* [4]. Although, there are various working fluids (molten salts, synthetic oil) that can be used as a heat transfer fluid (HTF) in the collector loop. However, such fluids are not suitable due to their flammability and toxicity. Under such circumstances, nanofluids are more suitable HTF option for the solar collectors. He *et al.* [5] experimentally investigated the performance of a vacuum tube solar receiver using CNT-water and TiO₂-water. The Al₂O₃/therminol VP1 nanofluid was examined in a concentrated parabolic solar collector by Khullar *et al.* [6] and a comparison between experimental results of a conventional parabolic concentrating solar collector was presented. Nanoparticles of four various sizes with different volume concentrations were investigated in a flat plate collector by Mahian *et al.* [7]. Sajid and Ali [8] studied the application of nanofluids in various heat transfer devices such as, heat sinks, shell and tube heat exchangers and plate type heat exchangers. Different experimental and numerical validated correlations have been assessed and compared. A numerical model of parabolic dish solar collector using two different nanofluids was developed and investigated from thermal and exergetic point of views [9]. The performance of PV/thermal solar collector was analysed by considering influence of lower and upper reflector and water based nanofluid [10]. They concluded that outlet temperature of water increased by 0.44% using nanofluid as a cooling medium. Laaraba [11] studied numerically the performance of flat plate solar thermal collector by adding partitions to the glazing wall. It was found that this addition reduced the thermal losses to the surroundings because of the decrease in Nusselt number. Daily performance of solar dish collector under different inlet temperature levels was studied by Pavlović *et al.* [12]. Collector thermal efficiency decreased between 67.36% and 54.65% with rise in temperature from 823-523 K. In contrast to individual Brayton or Rankine cycle, the combined cycles have received great attention because of their higher thermal efficiency in the design of power plants. The integration of combined gas cycle with solar energy is a cheaper way to harness solar thermal power [13], even at low solar input. Spelling *et al.* [14] conducted a thermo-economic optimization of combined power plant integrated with solar system. A detailed Second law efficiency investigation of combined cycle (ORC) integrated to a parabolic trough solar collector using seven different refrigerants was performed by Al-Sulaimen [15]. The exergy analysis of solar systems was conducted by Dincer and Rosen [16]. A tri-generation ORC was investigated from exergoenvironmental point of view by Ahmadi *et al.* [17], while a small scale integrated hydrogen and power generation system was exergo-economically analyzed by Caliskan *et al.* [18]. Parham *et al.* [19] accomplished a comprehensive thermodynamic and environmental analysis of a multi-production system having ORC, internal heat exchanger, open absorption heat transformation and an electrolyser. Hydrogen can be used as a fuel and offers exceptional advantages helping hydrogen to become one of the most important energy carrier in the future [20]. Electric power can be generated by the utilization of hydrogen in fuel cells. Researchers [21, 22] explored hydrogen for the purpose of friendly ecology and clean fuel. Various solar integrated hydrogen generation systems were examined by the researchers [23, 24]. The most effective

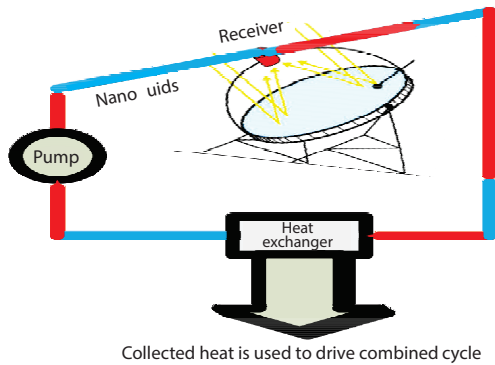


Figure 2. Solar dish collector with receiver

enters to the gas turbine at point – 3 for useful work. The pressure of the hot air is decreased by-passing through the gas turbine and it enters to the heat exchanger – 1 of the steam cycle. The temperature of the hot air at point – 4 is high enough to further heat the working fluid of the steam cycle. This high pressure high temperature steam is used to drive the high pressure steam, generating power output and steam expands at point – 6 and after again reheating, moves to the steam turbine – 2 for producing electricity. The maximum portion of power from turbine is used for buildings at state point – 30, whereas, small part is fed into the electrolyzer at point – 31 for hydrogen production. The steam becomes saturated liquid by-passing through condenser between state points – 8 and 9, while pump – 1 between state points – 9 and 10 pumps the saturated liquid back towards the steam turbine – 1 for recycling.

The air leaving the heat exchanger at state – 11 has relatively high temperature to power a single effect absorption chiller. The lithium bromide/water mixture is used in absorption cycle. At states – 15-17 solution is a weak, while, at states – 12-14 it is strong. The weak solution at point – 15 is compressed by the pump and after heating via heat exchanger – 2, it enters to the generator. The solution gets heated in the generator and splitting out the water vapors. The vapors at state – 18 go to the condenser, rejecting heat and then proceed to the refrigerant valve at point – 19 as a saturated liquid. It becomes saturated liquid vapor mixture t state – 20 after passing through the refrigerant valve and then this mixture enters into the evaporator, exchanging heat to the surroundings producing cooling effect and enters the absorber. The strong solution at state – 12 comes to the heat exchanger by giving heat to the weak solution and enters to the solution valve at – 13 and finally to the absorber where it absorbs the low grade vapor and reduces its temperature by discarding heat to the environment.

Table 1. Design parameters for single effect absorption system [26]

Parameter	Value
Capacity	1001 [kW]
Evaporator temperature	282 [K]
Exit temperature of generator solution	342 [K]
Exit temperature of generator vapor	338.8 [K]
Solution heat exchanger exit temperature	334.8 [K]
Heat exchanger effectiveness	70 [%]
Pump efficiency	100 [%]

effect absorption cycle for electricity, hydrogen production and cooling. The heat gained by the absorber tube of PDSC depicted in fig. 2, is transferred to the HTF and then as a useful heat to the heat exchanger A of the Brayton cycle. In a combined cycle power plant (CCPP), work is done in two-stages, air is working fluid in Brayton cycle and water is used in steam cycle. In heat exchanger A , heat of the nanofluids from collector is transferred to the air circulating in the gas cycle. The gas compressor between states points – 32 and 33 compresses this air to increase its pressure and temperature and then

Methodology

This section presents the methodology to solve the mathematical models of the solar integrated multigenerational system. The integrated system consists of the parabolic dish collector with nanofluids as a HTF, combined gas cycle, single effect lithium bromide absorption cycle chiller and hydrogen production system. The parametric

analysis are conducted using engineering equation solver. Assumptions consider for the solar integrated multigenerational system are, pressure drop in pipes and heat exchanger is negligible with zero heat transfer to the surroundings. Steady-state conditions are considered. Ambient temperature is 300 K, while receiver inlet temperature is 350 K. The design parameters for single effect absorption system, combined cycle and PDSC are given tabs. 1-3, respectively.

Table 2. Input parameters for combined cycle [30, 31]

Ambient temperature	300 [K]
Ambient pressure	100 [kPa]
Isentropic efficiency of compressor	80 [%]
Isentropic efficiency of pump	80 [%]
Isentropic efficiency of gas turbine	80%
Steam turbine isentropic efficiency	80 [%]
First steam turbine inlet pressure	6000 [kPa] [31]
Compressor outlet pressure	700 [kPa]
Condenser inlet pressure	10 [kPa]
Second steam turbine inlet pressure	1000 [kPa] [31]
Gas turbine exit temperature	100 [kPa]
Second steam turbine inlet temperature	741 [K]

Table 3. Input data used for PDSC [20, 32]

Optical efficiency	η_0	85 [%] [20]
Thermal conductivity	k	15 Wm ⁻¹ K ⁻¹
Emissivity of receiver	ϵ_r	90 [%]
Mass-flow rate	\dot{m}	0.06 [kgs ⁻¹]
Solar radiation	G_b	1000 [Wm ⁻²]
Inlet temperature	T_{in}	350 [K]
Receiver temperature	T_r	540 [K]
Wind speed	V_{air}	1 [ms ⁻¹]
Receiver outer diameter	D_{ro}	0.15 [m]
Receiver inner diameter	D_{ri}	0.015 [m]
Dish radius	R	2 [m]
Length of receiver	L	15 [m]
Temperature of the sun	T_s	5700 [K] [32]

Nanofluids properties

The nanofluids considered in the present study are Fe₂O₃/therminol VP1, SiO₂/therminol VP1, and Cu/therminol VP. The thermophysical properties of the nanofluids are higher in comparison base fluids therefore, they have maximum rate of heat transfer. The properties of the nanofluids are taken from [1, 20] and are presented tab. 4. A higher concentration is needed for the specification of nanofluid properties to achieve correct results of the simulation model. Nanoparticles concentration ratio, temperature and thermophysical properties of base fluid highly effect the thermophysical properties of nanofluids.

The volumetric fraction of nanoparticles is 2% to form nanofluids. The specific heat capacity and density of the nanofluids can be determined as suggested [33, 34]:

$$\rho_{nf} = \rho_{bf} (1 - \phi) + \rho_{np} \phi \tag{1}$$

$$C_{p,nf} = \frac{\rho_{bf} (1 - \phi)}{\rho_{nf}} C_{p,bf} + \frac{\rho_{np} \phi}{\rho_{np}} C_{p,np} \tag{2}$$

Table 4. Different properties of nanoparticles [1, 20]

Property	Cu	SiO ₂	Fe ₂ O ₃
Thermal conductivity [Wm ⁻¹ K ⁻¹]	400	1.4	5.38
Specific heat capacity [Jkg ⁻¹ K ⁻¹]	385	745	726.9
Density [kgm ⁻³]	8933	2220	5240

The viscosity, thermal diffusivity and thermal conductivity of the nanofluids can be calculated using equations as given [32, 26]:

$$\mu_{nf} = \mu_{bf} (1 + 2.5\phi + 6.5\phi^2) \quad (3)$$

$$\alpha_{nf} = \frac{k_{nf}}{(\rho C_p)_{nf}} \quad (4)$$

$$k_{nf} = \frac{k_{np} + 2k_{bf} - 2\phi(k_{bf} - k_{np})}{\frac{k_{np}}{k_{bf}} + 2 + \frac{k_{bf} - k_{np}}{k_{bf}}\phi} \quad (5)$$

Parabolic dish solar collector (PDSC)

The concentrated solar power technology used in this study is parabolic dish system and the receiver model is taken from [32].

Energy efficiency of the dish receiver and useful energy can be calculated:

$$\eta_{en,PDSC} = \frac{Q_u}{Q_{sun}} \quad (6)$$

$$Q_u = Q_r - Q_l \quad (7)$$

$$Q_l = U_L A_r (T_r - T_0) \quad (8)$$

where Q_r is the solar beam radiation falling on the collector, while Q_l – the heat loss from the receiver.

The useful heat gain can be found:

$$Q_u = \dot{m} C_p (T_{out} - T_{in}) \quad (9)$$

Amount of useful heat can also be found:

$$Q_u = F_r A_r \left[\left(S - \frac{A_r}{A_a} \right) U_L (T_{in} - T_a) \right] \quad (10)$$

The available solar energy is the combination of beam intensity and aperture area:

$$Q_{sun} = G_b A_a \quad (11)$$

Exergy analysis

The maximum possible work potential that is produced by parabolic dish collector is found by conducting exergy analysis. The exergy efficiency can be derived by using exergy balance of a solar receiver:

$$\sum \dot{E}_{x,in} - \sum \dot{E}_{x,out} - \sum \dot{E}_{x,loss} - \sum \dot{E}_{x,change} - \sum \dot{E}_{x,des} = 0 \quad (12)$$

Overall energy and exergy efficiencies of integrated system can be find:

$$\eta_{en,ov} = \frac{\dot{W}_{net}}{\dot{Q}_{solar}} \quad (13)$$

where Q_{solar} can be found from [34]:

$$\eta_{Ex,ov} = \frac{\dot{W}_{net}}{\dot{E}_{x,solar}} \quad (14)$$

Petela model is used to find out solar exergy:

$$\dot{E}_{x,solar} = G_b A_a \eta_{pet} \quad (15)$$

$$\eta_{pet} = \left[1 - \frac{4T_0}{3T_{Sun}} + \frac{1}{3} \left(\frac{T_0}{T_{Sun}} \right)^4 \right] \quad (16)$$

The equations used to model the combined power cycle analysis and single effect absorption system are taken from [30, 36], respectively and due to the space limitations cannot be presented here.

Electrolyzer and exergo-environmental analysis

The mathematical modelling of electrolyser is important to assess the rate of hydrogen produced through electrolysis process and equations that are used to investigate the electrolyzer have adopted from [20]. Moreover, environmental analysis has received a great attention in a past few years as it determines whether the investigated system is eco-friendly or not, based on the rate of total exergy destruction, exergetic efficiency and exergy input and output [22]. The major exergo-environmental parameters are taken from [19, 37] and will be discussed in results and discussion section only because of the space limitations.

Results and discussion

The present section of the work gives the results in detail obtained by simulation of the solar integrated multigenerational system. The results are authenticated with the previous studies and presented in tabs. 5 and 6. For parabolic dish system, energy efficiency of

Table 5. Validation with reference [32]

Material	η_{en} [%] PDSC
[32]	68.42
Fe ₂ O ₃ /therminol VP1	71.23
SiO ₂ /therminol VP1	70.22
Cu/therminol VP1	68.3

Table 6. Thermodynamic properties of the SEAS: present model (a), reference (b) [26] for SEAS

State point	P [kPa]		T [K]		h [kJkg ⁻¹]		s [kJkg ⁻¹ K ⁻¹]		x [% LiBr]	
	a	b	a	b	a	b	a	b	a	b
12	4.82	4.81	343	344	163.2	164.8	0.42	0.43	0.5694	0.5694
13	4.82	4.81	316.3	317.1	89.76	89.76	0.2548	0.26	0.5694	0.5694
14	1	1	313.7	313.5	89.76	89.76	0.2381	0.24	0.5694	0.5694
15	1	1	304.8	305	69.26	69.96	0.2079	0.21	0.5225	0.5225
16	4.82	4.81	304.8	305	69.26	69.96	0.2093	0.21	0.5225	0.5225
17	4.82	4.81	334.8	337.4	132.8	138.9	0.4069	0.43	0.5225	0.5225
18	4.82	4.81	338.8	341.3	2624	2627	8.602	8.62	0	0
19	4.82	4.81	305.4	305.4	135.1	134.8	0.4673	0.47	0	0
20	1	1	280.2	280	135.1	134.8	0.483	0.48	0	0
21	1	1	280.2	280	2513	2514	8.97	8.97	0	0

the receiver is almost near to the value given by Ngo [32], whereas, single effect absorption system is validated with the reference [26]. The mass-flow rate of the working fluid in the solar receiver is a vital parameter, which effects the efficiency of solar thermal power plants. The fig. 3 is the graphical representation of the influence of mass-flow rate of three different nanofluids and their impact on the overall exergy and energy efficiencies of the integrated system. The SiO_2 /therminol VP1 has the highest values of integrated energy and exergy efficiencies, increases from 32.13-39.03% and 34.5-41.98%, respectively. The Cu/therminol VP 1 has the lowest efficiency values amongst the investigated nanofluids, varying from 28.08-37.93% for overall energy efficiency, whereas, between 30.2% and 40.79% for overall exergy efficiency. Exergo-environmental impact coefficient, C_{ei} , and impact index, θ_{ei} , of the three nanofluids are assessed for different values of mass-flow rates. Higher values of above said performance parameters are obtained at lower mass-flow rates as shown in fig. 4. There is a rapid decrease in the values of C_{ei} and θ_{ei} between mass-flow rates of 0.1 kg/s and 0.3 kg per second and after 0.3-0.7 a less variation has been noticed. The C_{ei} exergoenvironmental impact coefficient is associated with the exergetic efficiency and C_{ei} increases when exergetic efficiency will reduce. The decrease in the C_{ei} values in present system contributes to rise the exergy efficiency which is much needed and better for environmental point of view. Exergoenvironmental impact index, θ_{ei} , is basically the product of exergoenvironmental impact coefficient and impact factor. Exergoenvironmental impact index, θ_{ei} , tells about the system under study, is whether or not damages the surroundings. Its value should be low for safer environment and in our study the θ_{ei} of solar thermal system working on three different nanofluids is reducing that reflects that the system under consideration is quite safer for the environment. The overall performance of the integrated system working on three different nanofluids has been examined at various ambient temperatures. At higher ambient temperatures, the system exhibits better productivity because the heat production rate and network output will be maximum at higher ambient conditions. The SiO_2 /VP1 has the maximum overall first and second law efficiencies, 38.79% and 41.72%, accordingly among the other nanofluids at ambient temperature of 300 K as seen in figs. 5. and 6 represents the influence of change in the ambient temperature on work output and hydrogen production rate of integrated system. The maximum net power production (almost 80%) is fed in to the grid for power, whereas, only 20% is used by the electrolyser for hydrogen production. According to the

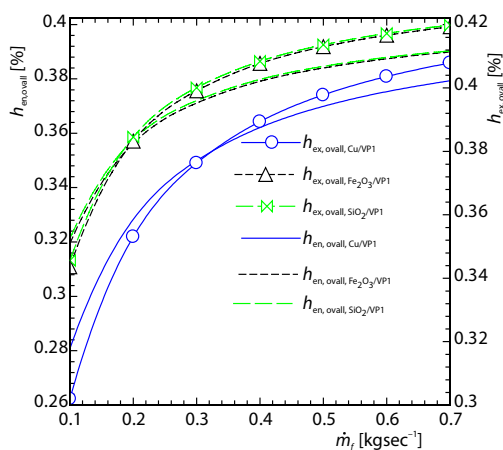


Figure 3. Mass-flow rate impact on integrated system efficiencies

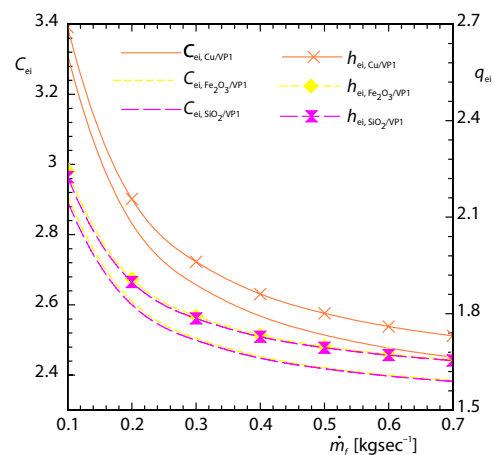


Figure 4. Comparison of C_{ei} and θ_{ei}

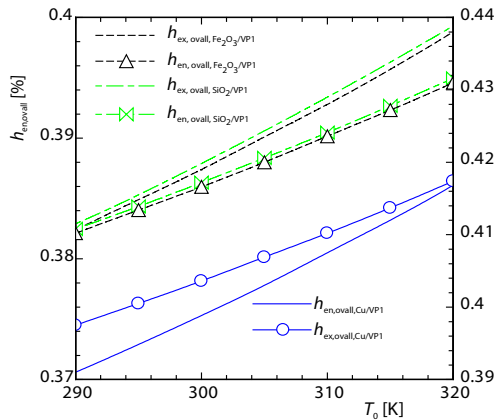


Figure 5. Comparison of integrated system efficiencies

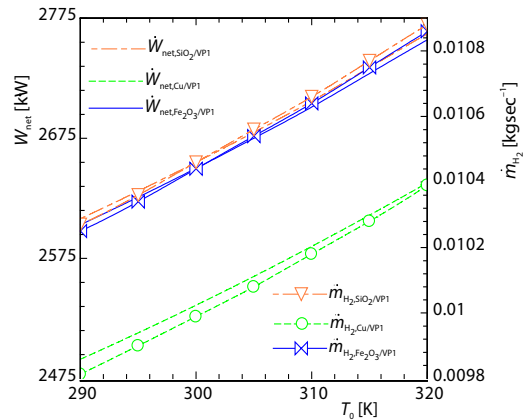


Figure 6. Comparison of net power and hydrogen production rate

tab. 6, the specific heat capacity of SiO_2 is greater (almost 745 J/kgK), therefore, this nanofluid is capable to produce maximum workout put as compared to the other two nanofluids.

The influence of the inlet temperature of HTF in solar receiver is plotted against exergo-environmental impact improvement, θ_{eii} , and exergetic sustainability index, θ_{est} , as given by fig. 7. The greater value of inlet temperature of HTF causes the surface temperature of collector to be rise that ultimately increases the rate of exergy destruction. Because of this reason, useful heat as well as workout put decreases. Therefore, the maximum value of θ_{eii} and θ_{est} is obtained at lower inlet temperature (350 K). The integrated system efficiencies vs. the inlet temperature are also plotted in fig. 8. The overall energy and exergy efficiencies of three nanofluids are varied from 38.79% and 38.43%, 41.72-41.34% for $\text{SiO}_2/\text{VP1}$, 38.74-38.43% and 41.66-41.28% for $\text{Fe}_2\text{O}_3/\text{VP1}$, and 37.53-37.19% and 40.36-40% for $\text{Cu}/\text{VP1}$, respectively. The influence of variation in DNI from 500-1000 Wm^2 on integrated system efficiencies at constant ambient temperature and mass-flow rate is plotted in fig. 9.

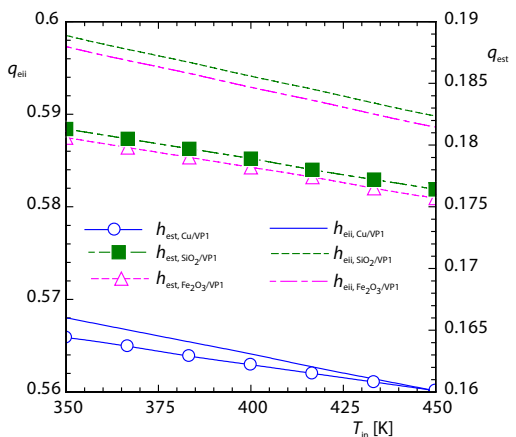


Figure 7. Inlet temperature effect on θ_{eii} and θ_{est}

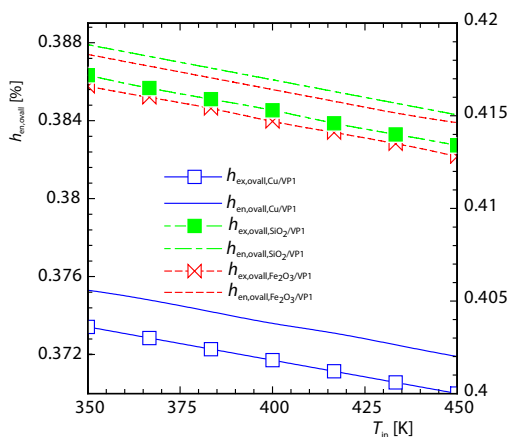


Figure 8. Inlet temperature influence on integrated system efficiencies

Solar radiations play an important role in the performance of integrated solar thermal power plants as areas have higher solar irradiations are feasible for the installation of power

plants. Higher solar irradiation intensity falling on the collector gives maximum amount of heat carried by the HTF circulating in the collector loop that ultimately contributes the higher outlet temperature [20]. Finally, network output is enhanced. The increase in the energetic and exergetic efficiencies for $\text{SiO}_2/\text{VP1}$ is almost linear, from 33.37-38.79% and 35.89-41.72%, respectively.

The amount of net work out is directly related with increase in the solar intensity and hydrogen production rate depends upon power output. Therefore, maximum heat production rate gives higher work output and hydrogen as well. The fig. 10 shows the influence of increase in solar radiations on the rate of hydrogen production and exergo-environmental impact factor, f_{ei} . The hydrogen production rates for three therminol-VP1 based nanofluids are increased linearly with the solar intensity. However, exergo-environmental impact factor is noticed to be reduced as DNI increases.

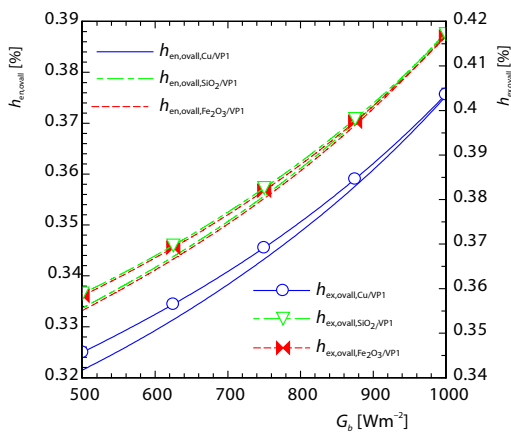


Figure 9. Solar irradiation impact on integrated system efficiencies

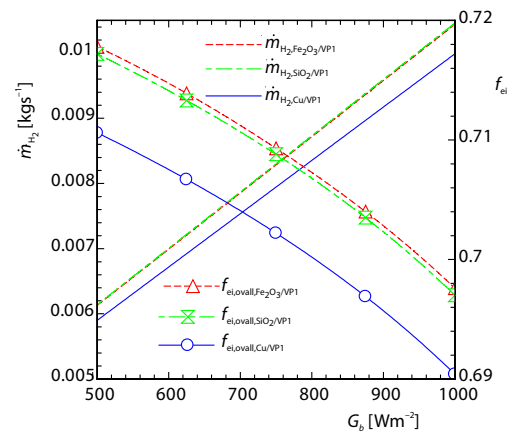


Figure 10. Effect of solar irradiation on f_{ei} and \dot{m}_{H_2}

The total rate of exergy destruction decreases at higher values of DNI that further helps to decrease the exergo-environmental impact factor and it is very helpful to enhance the system's performance [37]. According to the environmental point of view, f_{ei} value approaching to zero is better for the environment and in present study, values of, f_{ei} for all the three nanofluids are gradually moving towards the zero. Figure 11 depicts the effect of rise in the concentration of nanoparticles on overall exergy efficiency of the integrated solar thermal system. It can be observed that the efficiency enhances significantly by adding nanoparticles concentrations. The $\text{SiO}_2/\text{VP1}$ and $\text{Cu}/\text{VP1}$ have the highest and the lowest values, respectively amongst the examined fluids.

The thermal conductivity of the nanofluids is observed to be decreased while density is going to be enhanced by adding the nanoparticles concentration as plotted in fig. 12. The variations in the density of nanofluids is also plotted against inlet temperature of the fluid, as seen in fig. 13.

According to the environmental point of view, f_{ei} value approaching to zero is better for the environment and in present study, values of, f_{ei} for all the three nanofluids are gradually moving towards the zero. Figure 11 depicts the effect of rise in the concentration of nanoparticles on overall exergy efficiency of the integrated solar thermal system. It can be observed that the efficiency enhances significantly by adding nanoparticles concentrations. The $\text{SiO}_2/\text{VP1}$ and $\text{Cu}/\text{VP1}$ have the highest and the lowest values, respectively, amongst the examined fluids. The

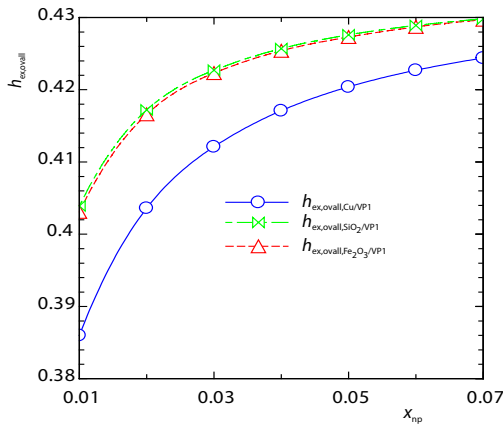


Figure 11. Comparison of integrated system exergy efficiency

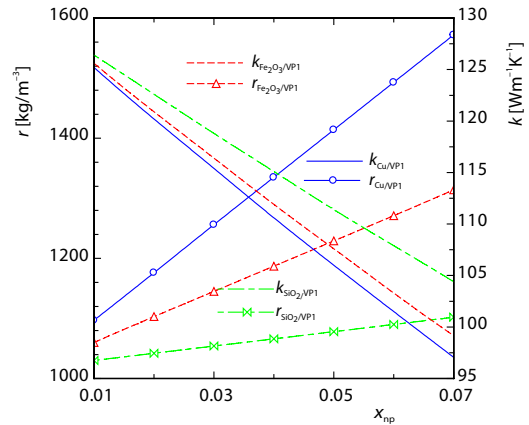


Figure 12. Variations in density and conductivity against % age concentration of nanofluids

thermal conductivity of the nanofluids is observed to be decreased while density is going to be enhanced by adding the nanoparticles concentration as plotted in fig. 12. The variations in the density of nanofluids is also plotted against inlet temperature of the fluid, as seen in fig. 13. The performance parameter of the three nanofluids is reduced when inlet temperature increases with Cu/VP1 has the highest density among the investigated nanofluids.

The impact of rise in the evaporator temperature on the energetic as well as exergetic COP is presented in fig. 14. The COP_{en} has increased, whereas, COP_{ex} moves in an opposite way as the evaporator temperature rises. The greater value of COP is obtained at higher evaporator and less generator temperatures but the trend of COP_{ex} is in an opposite way [33]. The influence of rise in the generator temperature between 320 K and 380 K reduces the COP from 0.875-0.797 as well as overall energy and exergy efficiencies from 40.31-39.34% and 43.35-42.3%, respectively at $T_{cond} = 305.4$ K and $T_{evp} = 281$ K and is shown in fig. 15. The reason behind is that increase in the T_{gen} also boosts the strong solution concentration by maximizing the flow ratio. This phenomenon causes the reduction of the absorption heat capacity. At the end, system integrated efficiencies and coefficient of performance are reduced [38].

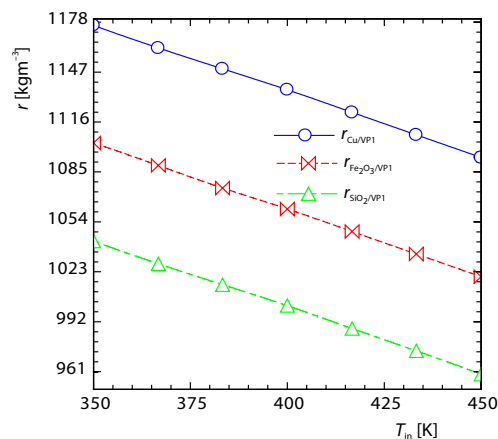


Figure 13. Variations in the densities of the nanofluids

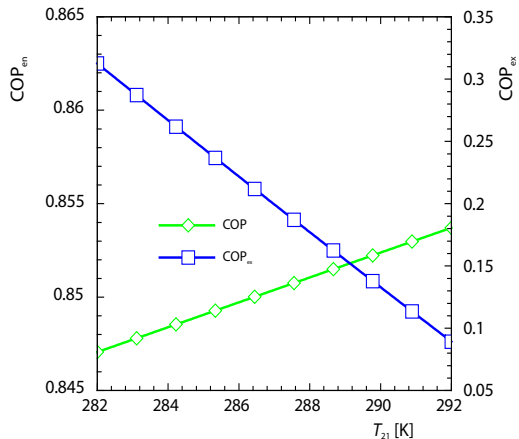


Figure 14. Evaporator temperature effect

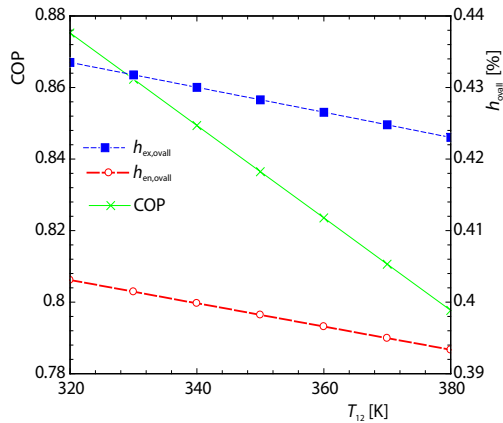


Figure 15. Generator temperature influence

to the Fe_2O_3 and 3.35% to Cu based nanofluids at 300 K and 1000 W/m^2 . Increase in mass rate of HTF from 0.1-0.3 kg/s results in substantial enhancement of integrated efficiencies, 24.60% for Cu/VP1, 16.15% for e_2O_3 /VP1, and 15.7% for SiO_2 /VP1 based nanofluids. However, from 0.3-0.7 kg/s, less increment is found in efficiency values, 8.40%, 5.06%, and 4.9%, respectively, for three mentioned oil based nanofluids. Densities of Cu/VP1, Fe_2O_3 /VP1, and SiO_2 /VP1 are increased to almost 43%, 23%, and 7%, respectively, with rise in nanoparticles concentration. Furthermore, rise in the inlet temperature of the working fluid in collector reduces the density for SiO_2 /VP1, Fe_2O_3 /VP1, and Cu/VP1 from 1042-959 kg/m^3 , 1103-1020 kg/m^3 , and 1176-1094 kg/m^3 , respectively, because of the rise in the exergy losses from the receiver surface. The increase in the evaporator temperature also increase the COP of the SEAS, while coefficient of performance decreases with rise in the generator temperature.

Nomenclature

A_a – area of aperture, [m^2]
 A_r – area of receiver, [m^2]
 C_p – specific heat capacity, [$Jkg^{-1}K^{-1}$]
 $\dot{E}_{x,in}$ – exergy rate, [kW]
 F_r – heat removal factor
 h – specific enthalpy, [$kJkg^{-1}$]
 h_{con} – convection heat transfer, [$Wm^{-2}K^{-1}$]
 G_b – solar radiation, [Wm^{-2}]
 k – thermal conductivity, [$Wm^{-2}K^{-1}$]
 Q_u – useful heat, [kW]
 \dot{m} – mass-flow rate, [$kg s^{-1}$]
 S – absorbed solar radiation, [Wm^{-2}]
 s – entropy, [$kJkg^{-1}K^{-1}$]
 T_r – temperature of receiver, [K]
 T_0 – ambient temperature, [K]
 U_L – overall heat loss, [$Wm^{-2}K^{-1}$]
 \dot{W} – net work output, [kW]

Greek symbols

α – thermal diffusivity, [m^2s^{-1}]
 η – efficiency, [%]
 ρ – density, [kgm^{-3}]

Conclusions

The current study evaluates and compares the performance of parabolic dish solar assisted multigenerational system using three different nanofluids. The multigenerational system includes combined power cycle for electricity, an electrolyser for hydrogen production and SEAS (LiBr-water) to produce cooling effect. Furthermore, exergoenvironmental analyses are also conducted in details to assess the effect of exergy losses from the integrated system. The core findings of the study are concluded here. The integrated system energy efficiency of SiO_2 based nanofluid is 38.79% and witnessed to be the higher 0.12% as compared

ρ_{nf} – density of nanofluid, [kgm^{-3}]
 ϕ – nanoparticles, [%age]

Acronyms

elec – electrolyzer
 PD – parabolic dish
 PDSC – parabolic dish solar collector
 SEAS – single effect absorption system

Subscripts

bf – basefluid
 des – destruction
 en – energy
 l – loss
 nf – nanofluid
 np – nanoparticle
 ov – overall
 pet – petela
 r – radiation

References

- [1] Loni, R., et al., Thermodynamic Analysis of a Solar Dish Receiver Using Different Nanofluids, *Energy*, 133 (2017), Aug., pp. 749-760
- [2] ***, IRENA, Renewable Power Generation Costs in 2012: an Overview, Abu Dhabi, United Arab Emirates, 2012
- [3] Le Roux, W. G., et al., The Efficiency of an Open-Cavity Tubular Solar Receiver for a Small-Scale Solar Thermal Brayton Cycle: *Energy Convers Manag.*, 84 (2014), Aug., pp. 457-70
- [4] Qiu, K., et al., Simulation and Experimental Study of an Air Tube-Cavity Solar Receiver: *Energy Convers Manag.*, 103 (2015), Oct., pp. 847-58
- [5] He, Y., et al., Experimental Study on the Light-Heat Conversion Characteristics of Nanofluids: *Nanoscience and Nanotechnology Letters*, 3 (2011), 4, pp. 494-96
- [6] Khullar, V., et al., Solar Energy Harvesting Using Nanofluids-Based Concentrating Solar Collector: *Journal of Nanotechnology in Engineering and Medicine*, 3 (2012), 3, 031003
- [7] Mahian, O., et al., Entropy Generation during Al_2O_3 /Water Nanofluid-Flow in a Solar Collector: Effects of Tube Roughness, Nanoparticle Size, and Different Thermophysical Models: *Int. J. Heat Mass Transfer*, 78 (2014), Nov., pp. 64-75
- [8] Sajid, M. U., Ali, H. M., Recent Advances in Application of Nanofluids in Heat Transfer Devices: *A Critical Review, Renewable and Sustainable Energy Reviews*, 103 (2019), Apr., pp. 556-592
- [9] Pavlović, S., et al., Thermal and Exergetic Investigation of a Solar Dish Collector Operating with Mono and Hybrid Nanofluids: *Thermal Science*, 22 (2018), Suppl., pp. S1383-S1393
- [10] Ahmed, O. K., Bawa, S. M., The Combined Effect of Nanofluid and Reflective Mirrors on the Performance of PV/Thermal Solar Collector: *Thermal Science*, 23 (2018), 2A, pp. 573-587
- [11] Laaraba, A., Numerical Study of Heat Transfer in a Flat Plat Thermal Solar Collector with Partitions Attached to Its Glazing: *Thermal Science*, 23 (2018), 2B, pp. 1057-1084
- [12] Pavlović, S., et al., Daily Performance of a Solar Dish Collector: *Thermal Science*, 23 (2018), 3, pp. 2107-2115
- [13] Montes, M. J., et al., Performance of a Direct Steam Generation Solar Thermal Power Plant for Electricity Production as a Function of the Solar Multiple: *Solar Energy*, 83 (2009), 5, pp. 679-689
- [14] Spelling, J., et al., Thermoeconomic Optimization of a Combined-Cycle Solar Tower Power Plant: *Energy, Elsevier Ltd.*, 41 (2012), 1, pp. 113-120
- [15] Al-Sulaiman, F. A., Exergy Analysis of Parabolic trough Solar Collectors Integrated with Combined Steam and Organic Rankine Cycles: *Energy Conversion and Management, Elsevier Ltd.*, 77 (2014), Jan., pp. 441-449
- [16] Dincer, I., Rosen, M. A., *Exergy, Energy, Environment and Sustainable Development*, Elsevier, Oxford, UK, 2007
- [17] Ahmadi, P., et al., Exergo-Environmental Analysis of an Integrated Organic Rankine Cycle for Trigeneration: *Energy Convers Manag.*, 64 (2012), Dec., pp. 447-53
- [18] Caliskan, H., et al., Exergoeconomic and Environmental Impact Analyses of a Renewable Energy Based Hydrogen Production System: *Int. J. Hydrogen Energy*, 38 (2013), 14, pp. 6104-11
- [19] Parham, K., et al., Energy, Exergy and Environmental Analysis of a Novel Combined System Producing Power, Water and Hydrogen: *Energy*, 134 (2017), Sept., pp. 882-892
- [20] Abid, M. et al., Solar assisted multi-generation system using nanofluids: A comparative analysis: *International Journal of Hydrogen Energy*, 42 (2017), 33, pp. 21429-21442
- [21] Ratlamwala, T. A. H., et al., Performance Analysis of a New Designed PEM Fuel Cell, *Int. J. Energy Res.*, 36 (2012), 11, pp. 1121-1132
- [22] Midilli, A., Dincer, I., Development of Some Exergetic Parameters for PEM Fuel Cells for Measuring Environmental Impact and Sustainability, *Int. J. Hydrogen Energy*, 34 (2009), 9, pp. 3858-3872
- [23] Yilanci, A., et al., Performance Analysis of a PEM Fuel Cell Unit in a Solar Hydrogen System, *Int. J. Hydrogen Energy*, 33 (2008), 24, pp. 7538-7552
- [24] Hollmuller, P., et al., Evaluation of a 5 kW Photo-Voltaic Hydrogen Production and Storage Installation for a Residential Home in Switzerland, *Int. J. Hydrogen Energy*, 25 (2000), 2, pp. 97-109
- [25] Kalinci, Y., et al., Energy and Exergy Analyses of a Hybrid Hydrogen Energy System: A Case Study for Bozcaada, *Int. J. Hydrogen Energy*, 42 (2016), 4, pp. 2492-2503
- [26] Ratlamwala, T. A. H., Abid, M., Performance Analysis of Solar Assisted Multi-Effect Absorption Cooling Systems Using Nanofluids: A Comparative Analysis, *International Journal of Energy Research*, 42 (2018), 9, pp. 2901-15

- [27] Bahman, A. M. K., Modelling of Solar-Powered Single-Effect Absorption Cooling System and Supermarket Refrigeration/HVAC System, Ph. D. thesis, University of South Florida, Tampa, Fla., USA, 2011
- [28] Asdrubali, F., et al., Solar Cooling with Small-Size Absorption Chillers: Different Solutions for Summer Air Conditioning, *Proceedings, XIII European Conference IIR – Centro Studi Galileo, Milano, Italy, 2009*, pp. 12-13
- [29] De Vega, M., et al., Performance of a LiBr-water Absorption Chiller Operating with Plate Heat Exchangers, *Energy Conversion and Management, 47* (2006), 18-19, pp. 3393-3407
- [30] Sheykhrou, H., Jafarmadar, S., Analysis of a Combined Power and Ejector-Refrigeration Cycle Based on Solar Energy: Iranian Journal of Science and Technology, *Transactions of Mechanical Engineering, 40* (2016), 1, pp. 57-67
- [31] Cengel, Y. A., Boles, M. A., *Thermodynamics: An Engineering Approach, 7th ed.*, McGraw-Hill, New York, USA, 2017
- [32] Ngo, L. C., et al., Exergetic Analysis and Optimisation of a Parabolic Dish Collector for Low Power Application, *Proceedings, Postgraduate Symposium 2012, Stellenbosch, Sout Africa, Centre for Renewable and Sustainable Energy Studies (CRSES), 2012*
- [33] Khanafer, K., Vafai, K., A Critical Synthesis of Thermophysical Characteristics of Nanofluids, *Int. J. Heat. Mass Transf, 54* (2011), 19-20, pp. 4410-4428
- [34] Khan, M. S., et al., Energy, Exergy and Economic Feasibility Analyses of a 60 MW Conventional Steam Power Plant Integrated with Parabolic Trough Solar Collectors Using Nanofluids: Iranian Journal of Science and Technology, *Transactions of Mechanical Engineering, 43* (2018), Suppl. 1, pp. S193-S209
- [35] Colburn, A. P., A Method for Correlating Forced Convection Heat Transfer data and a Comparison with Fluid Friction, *Trans. Am. Inst. Chem. Engrs.*, 29 (1933), pp. 174-210
- [36] Gebreslassie, B. H., et al., Exergy Analysis of Multieffect Water-LiBr Absorption Systems: From Half to Triple Effect, *Renew Energy, 35* (2010), 8, pp. 1773-1782
- [37] Ratlamwala, T. A. H., et al., Exergetic and Environmental Impact Assessment of an Integrated System for Utilization of Excess Power from Thermal Power Plant, in: *Causes, Impacts and Solutions to Global Warming*, Springer, New York, USA, 2013, pp. 803-824
- [38] Gomri, R., Second Law Comparison of Single Effect and Double Effect Vapour Absorption Refrigeration Systems, *Energy Conversion and Management, 50* (2009), 5, pp. 1279-1287